



## Article

# Size Distribution and Variation in Surface-Suspended Sediments in the North Passage Estuarine Turbidity Maximum of the Yangtze Estuary

Steve L. Zeh Assam <sup>1,\*</sup>, Yongping Chen <sup>1</sup>, Ao Chu <sup>2</sup>, Samuel Ukpong Okon <sup>3,4</sup>, Genide Anteilla L. M. <sup>1</sup> and Giresse Ze Eyezo'o <sup>1</sup>

<sup>1</sup> College of Harbor, Coastal and Offshore Engineering, Hohai University, Nanjing 210098, China; ypchen@hhu.edu.cn (Y.C.)

<sup>2</sup> Institute of Water Science and Technology, Hohai University, Nanjing 210098, China

<sup>3</sup> Institute of Port, Coastal and Offshore Engineering, Ocean College, Zhejiang University, Hangzhou 316021, China; samukpong@zju.edu.cn

<sup>4</sup> Suzhou Industrial Technological Research Institute of Zhejiang University, Suzhou 215163, China

\* Correspondence: stevezehassam@hhu.edu.cn

**Abstract:** One of the most important processes for mass movement in coastal areas is sediment transport; it plays a significant role in coastal morphology changes. This manuscript focuses on the distribution and variation in surface-suspended sediments in the North Passage of the Yangtze Estuary. Field data on surface-suspended sediment concentration (SSSC) and suspended particle size (SPS) were collected at fifteen hydrological sites over a period of three years, from 2016 to 2018. The main objective was to analyze the spatial and temporal patterns of sediment and particle size and their potential impact on the estuary. Results indicate that extreme weather events have an influence on the hydrological conditions and sediment dynamics of the area. The intensity and range of SSSC variation in the North Passage seem to be determined by the magnitude of the current velocity, while the sediment load significantly impacted the sediment distribution pattern. This study demonstrates that surface sediment dynamics can be used as a basis for understanding the spatiotemporal variation in estuarine turbidity maximum (ETM) in the North Passage of the Yangtze Estuary.

**Keywords:** Yangtze estuary; North Passage; surface-suspended sediment; particle size distribution; tidal phases



**Citation:** Assam, S.L.Z.; Chen, Y.; Chu, A.; Okon, S.U.; Anteilla L. M., G.; Eyezo'o, G.Z. Size Distribution and Variation in Surface-Suspended Sediments in the North Passage Estuarine Turbidity Maximum of the Yangtze Estuary. *Water* **2024**, *16*, 306. <https://doi.org/10.3390/w16020306>

Academic Editor: Yiannis Savvidis

Received: 8 December 2023

Revised: 28 December 2023

Accepted: 29 December 2023

Published: 17 January 2024



**Copyright:** © 2024 by the authors. Licensee MDPI, Basel, Switzerland. This article is an open access article distributed under the terms and conditions of the Creative Commons Attribution (CC BY) license (<https://creativecommons.org/licenses/by/4.0/>).

## 1. Introduction

Researchers have always focused on suspended sediments because of their importance in controlling estuarine sediment dynamics and reshaping geomorphological patterns [1,2]. Siltation of the navigation channel [3], pollution [4], and the formation of estuarine turbidity maximum (ETM) [5,6] are exacerbated by suspended sediments, owing to their intrinsic attributes such as adsorptive capacity, low density, particle sizes, and settling velocity. In the last few years, siltation of the navigational channel has been observed in many estuaries in China, including the Changjiang (Yangtze) Estuary [5,7,8], Yellow River Estuary [6,9], and Pearl River Estuary [10,11], raising significant environmental and ecological concerns. For instance, the estuarine turbidity maximum develops as a result of elevated suspended particulate matter (SPM) concentration at the interface between the river and the sea [12,13].

From an environmental point of view, ETM areas are mostly characterized by limited light penetration in the water column, increased turbidity, and reduced transparency [11,14]. These observations imply that there might be an alternative way to study ETM; surface water within a turbid zone is an important visual characteristic. Even so, it is only a qualitative assessment because the amount of turbidity and suspended sediment concentration (SSC) in the water column are unknown at this time.

Significant research efforts have focused on suspended and bed sediment to understand the mechanisms of sediment dynamics around the estuarine turbidity maximum using various approaches such as remote sensing [9,15–17], numerical modelling [18,19], and field data analysis [20,21]. For instance, Wu et al. [22,23] analyzed both bathymetric data and riverbed dunes to understand the morphological changes and sediment transport mechanism during floods in the Yangtze Estuary. More recently, Tang et al. [24] used multi-beam echo sounding and historical bathymetry datasets to access the decadal changes in riverbed volume and erosion/deposition patterns in the South Channel and South Passage of the Yangtze Estuary. Teng et al. [25] also investigated suspended sediment characteristics, particle size distribution, and current velocity in the Yangtze Estuary using remote sensing technology. Silva et al. [26,27] analyzed the morphology and SSC dynamics of a tide-dominated estuary in the Amazon River, while Yang et al. [21] studied suspended sediment concentration through field data analysis. Using an analogous method, Yun et al. [28] investigated the effect of SSC, tidal current, salinity, particle size distribution, turbulent kinetic energy, and Richardson number of suspended sediments. Han et al. [7] modelled fine sediment transport to understand the ETM. As a result of the above studies, the understanding of the mechanism behind suspended sediment dynamics has been significantly improved. Although previous remote sensing methods described the surface-suspended sediment distribution in the northern passage of the Yangtze Estuary [16,17], an improved understanding of important mechanisms associated with surface sediment dynamics is still necessary to understand and predict the dynamics behind the ETM formation. Most sedimentary processes, such as erosion [28], resuspension, siltation, and accretion, are related to the bed and suspended sediment.

While early grain size studies primarily focused on establishing links between sedimentary environments and summary statistics of grain size distribution, such as the mean, standard deviation, and skewness [29], this study aimed to extend the available understanding of turbidity maximum zone which is mainly linked and related to sediment dynamics. In this paper, we present our findings on the field investigation of the spatio-temporal distribution and variation in SSSC and SPS in the North Passage of the Yangtze Estuary and how extreme weather events influence the sediment dynamic and estuarine turbidity maximum of the area. Key characteristics connected with SPS and SSSC through mean and standard deviation at the North Passage ETM area are highlighted. The main objectives of this study are (i) to describe the impact of the hydrodynamics and environmental conditions on the SSSC and SPS variation and distribution, (ii) examine seasonal and annual variability of SSSC and SPS, (iii) elucidate the role of the tidal phases in the distribution and variation in SPS and SSSC, and (iv) locate and predict potential ETM spot and area through SSSC and SPS variation and distribution. The remaining part of this paper is organized as follows: Section 2 describes the study area and the methodology used for data collection. Section 3 presents the hydrological and hydrodynamic conditions of the North Passage during the three-year observation period from 2016 to 2018, highlighting the differences and similarities in the seasonal and annual variation and the distribution of SSSC and surface particle size. Discussions are presented in Section 4, as well as the SSSC and SPS variability under the influence of tidal phases while Section 5 provides important concluding remarks.

## 2. Methodology and General Conditions of the Study Area

### 2.1. Study Area

The Yangtze Estuary is a mesotidal estuary with a mean tidal range of 2.5 m. It is the third-largest river globally in terms of river discharge and sediment load, with a total length of 6300 km [30–32]. Excess river runoff transports a large amount of sediment into the estuary, modifying the wide estuarine delta. Using a sediment budget method, Zhu et al. [7,33] estimated the sediment load in the Yangtze Estuary to be 132 million metric tons per year (Mt/yr.), representing a 68% decrease from 1960 to 2019 [7]. The North

Passage of the Yangtze Estuary is illustrated in Figure 1b, where fifteen (15) stations were established and sampled for analysis.

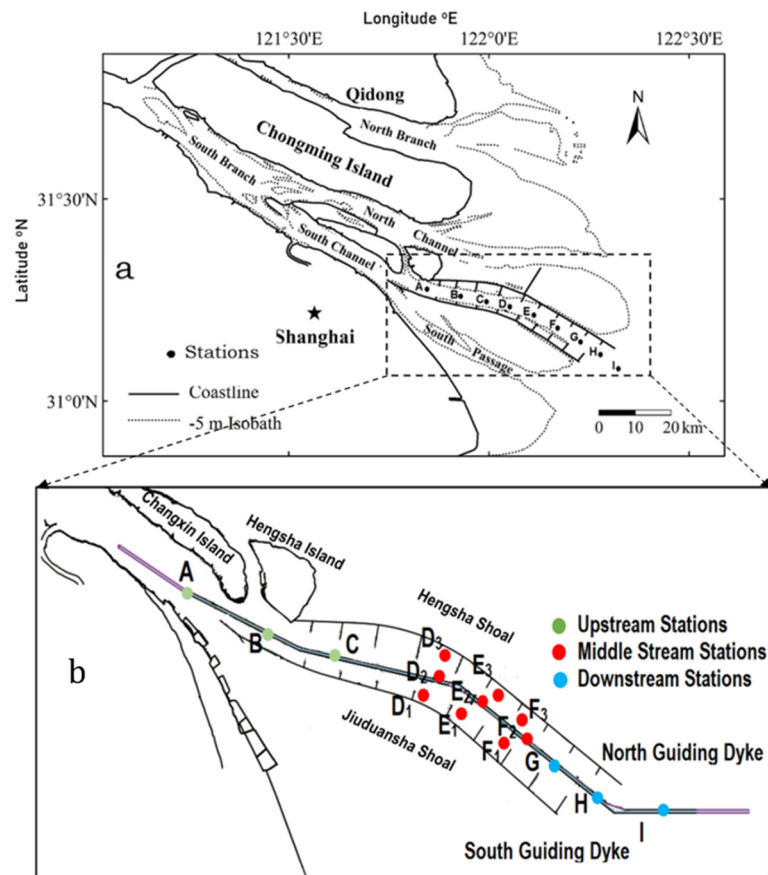


**Figure 1.** (a) General layout of the Yangtze Estuary; (b) location of the sampling stations in the channel.

As presented in Figure 1a, nine (9) primary stations were established along the main channel and marked from upstream to downstream as stations A, B, C, D, E, F, G, H, and I. These stations were further classified into the upstream stations comprising stations A, B, and C, the middle stream comprised of stations D, E, and F, and downstream stations comprised of stations G, H, and I. Each of the three middle stream stations (i.e., D, E, and F) was further subdivided into three sub-stations across the channel and denoted by red dots (see Figure 1b). Sub-stations D1, E1, and F1 were located along the southern border of the channel, sub-stations D2, E2, and F2 were located along the middle of the channel, and sub-stations D3, E3, and F3 were located along the northern border. For clarity purposes, sub-stations D1, D2, and D3 will be together referred to as cross-section 1 (CS1), sub-stations E1, E2, and E3 will be together referred to as cross-section 2 (CS2), and sub-stations F1, F2, and F3 will be together referred to as cross-section 3 (CS3). Notably, all the sub-stations across the middle stream were located at the high siltation spot in the North Passage. As earlier observed by previous research, the Yangtze Estuary shows a river regime pattern of three-stage bifurcation and four outlets entering the sea [30,31].

## 2.2. Methodology and Data Processing

It is noteworthy that this study used data from the “2016, 2017 and 2018 Annual Hydrographic Sediment chart set of the Yangtze River Estuary Water Environment Monitoring Centre.” Grain size analysis was conducted using a Mastersizer 2000 laser grain-size analyzer (Malvern Instruments, Malvern, UK) while the detection range was 0.02–2000  $\mu\text{m}$ . About 1 g of the sample was boiled in 10 mL of 10%  $\text{H}_2\text{O}_2$  for 10 min to remove the

organic matter. Then, about 10 mL of 10% HCl was added for another 10 min to ensure that carbonate was completely removed. The sample was subsequently rinsed in 1000 mL of distilled water for 24 h. A drop of 0.05 N  $(\text{NaPO}_3)_6$  was then added after carefully removing the supernatant. The sample was dispersed for 10 min in an ultrasonic bath before measurement [22,33]. The flow velocity and current direction were monitored hourly using an ADCP in addition to a flow velocity and current direction meter. Notably, water stratification was taken into account throughout the collection and processing of samples. WinRiver software was used to provide timely and accurate information on the water conditions at each depth of the water column using the information collected by the ADCP. The vector decomposition and synthesis method was used to find out the east west and north south components of the flow velocity at each measurement point, while the mean vertical flow velocity and mean flow direction were calculated by synthesizing the mean vertical flow velocity and mean flow direction according to the mean vertical flow velocity of each component. The technical specifications, requirements and regulations of the Yangtze River Estuary Waterway Management Bureau of the Ministry of Transportation of the People's Republic of China (PRC) and the Hydrographic and Water Resources Survey Bureau of the Yangtze River Estuary were strictly applied during the data collections and processing [27,34–41]. The Classification Standard for Dredged Rock and Soil [42,43] (i.e.,  $\leq 5 \mu\text{m}$ ,  $\leq 16 \mu\text{m}$ ,  $\leq 31 \mu\text{m}$  and  $\leq 62 \mu\text{m}$ ,  $\leq 75 \mu\text{m}$ ,  $\leq 100 \mu\text{m}$ ,  $\leq 125 \mu\text{m}$ ,  $\leq 250 \mu\text{m}$ ,  $\leq 500 \mu\text{m}$ ,  $\leq 1000 \mu\text{m}$ ) was applied for the grain size analysis.

In the computation of particle distribution parameters, particle-size distributions are commonly characterized by four distribution parameters: mean, standard deviation, skewness, and kurtosis [30,44]. In this study, the mean particle size diameter ( $D_{50}$ ), which characterizes the central part of the distribution, and the standard deviation (i.e., std), which indicates the distribution (i.e., the range) of the sediment particle size distribution, were considered. At each station, hourly suspended sediment concentration (SSC) and  $D_{50}$  data were measured across six different depths of the water column, 0.0  $H$ , 0.2  $H$ , 0.4  $H$ , 0.6  $H$ , 0.8  $H$ , and 1.0  $H$ , where  $H$  represents the total water depth in meters (m). In order to match the regular tidal cycle, 25 h of data during spring and neap tides for 2016, 2017, and 2018 were used for analysis (Table 1). Since the Yangtze River estuary is a tidal-dominated estuary, implying that the tidal effect is dominant, we assume that tides have a greater effect on estuaries than waves [45–47]. For this reason, the present study focused on the influence of tides on the surface sediment concentration and the particle size distribution during the four tidal periods (flood, high slack water, ebb and low slack water).

**Table 1.** Schedule time of samples.

		Spring Tides		Neap Tides	
		Start	End	Start	End
Summer	2016	21 July at 7 a.m.	22 July at 11 a.m.	27 July at 10 a.m.	28 July at 9 p.m.
	2017	10 July at 7 p.m.	11 July at 11 p.m.	18 July at 12 noon	19 July at 7 p.m.
	2018	14 August at 6 a.m.	15 August at 11 a.m.	6 August at 11 a.m.	7 August at 5 p.m.
Winter	2017	28 February at 7 p.m.	02 March at 00 p.m.	21 February at 12 noon	22nd February at 9 p.m.
	2018	30 January at 4 p.m.	31st January at 10 p.m.	8 February at 5 p.m.	9 February at 10 p.m.

### 3. Results

#### 3.1. Hydrological and Hydrodynamic Conditions of the North Passage of Yangtze Estuary

The average monthly discharge of  $32,795 \text{ m}^3\text{s}^{-1}$  was recorded in 2016, which subsequently decreased to  $29,626 \text{ m}^3\text{s}^{-1}$  and  $25,616 \text{ m}^3\text{s}^{-1}$  in 2017 and 2018, respectively. During the summer study period, the average daily river discharge recorded at Datong hydrological station showed higher values of  $63,250 \text{ m}^3\text{s}^{-1}$  and  $67,350 \text{ m}^3\text{s}^{-1}$  in 2016 compared to  $58,550 \text{ m}^3\text{s}^{-1}$  and  $67,050 \text{ m}^3\text{s}^{-1}$  recorded in 2017, as well as  $41,750 \text{ m}^3\text{s}^{-1}$  and  $38,700 \text{ m}^3\text{s}^{-1}$  recorded in 2018, for both neap and spring tides respectively. During the winter season, the daily river discharge was lower in 2017 compared to 2018.

The study showed a decline in the daily depth-averaged suspended sediment concentration (DASSC) values at the Datong station from  $0.12 \text{ kgm}^{-3}$  in 2016 to  $0.08 \text{ kgm}^{-3}$  in 2018. At the North Passage, the along-channel DASSC value of  $0.88 \text{ kgm}^{-3}$  was recorded in 2018, while the value of  $0.42 \text{ kgm}^{-3}$  was recorded in 2016, and  $0.36 \text{ kgm}^{-3}$  was recorded in 2017 (see Figure 2a). The DASSC at neap tide was  $0.34 \text{ kgm}^{-3}$  in 2017, which was twice the value observed in both 2016 and 2018. During the winter season, the neap tide values for 2017 and 2018 were about the same, measuring  $0.13 \text{ kgm}^{-3}$  and  $0.15 \text{ kgm}^{-3}$ , respectively. However, these values were four times lower than the spring tide value observed in 2017.

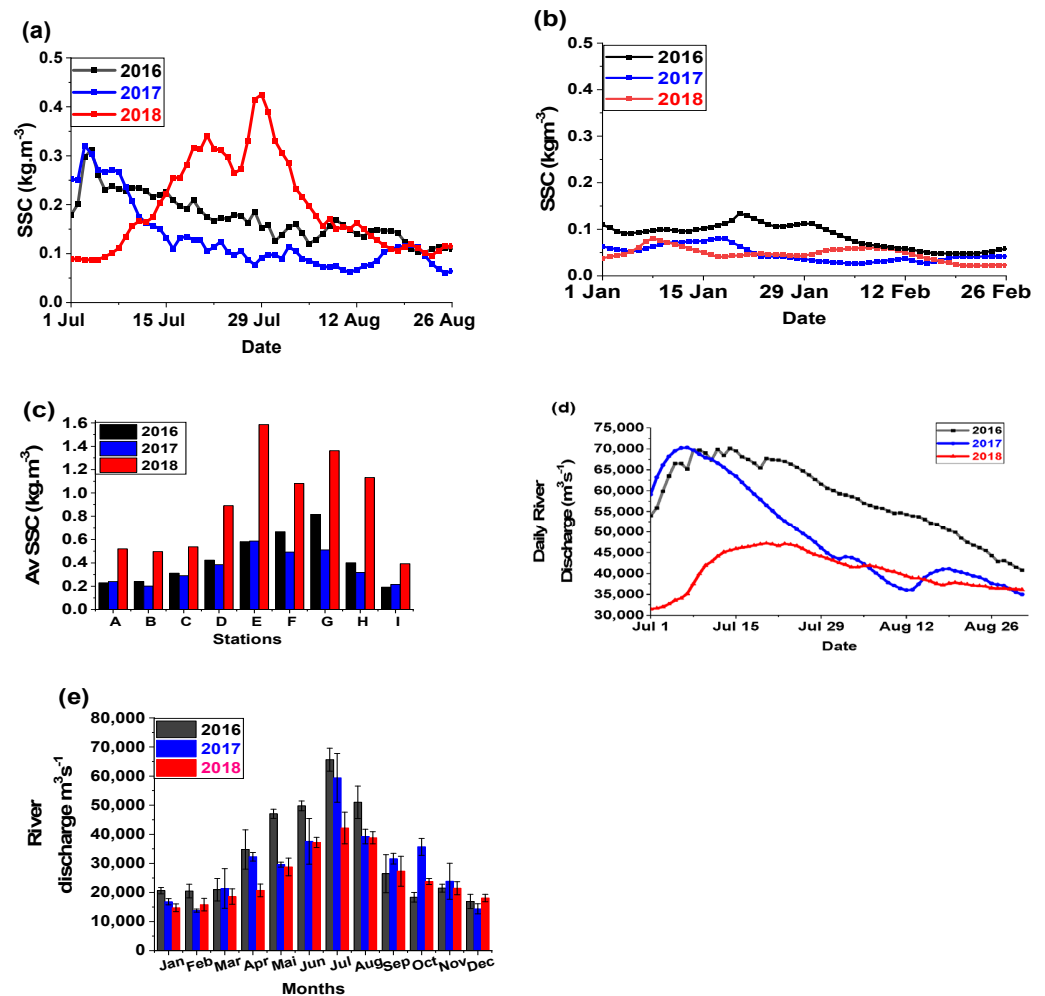


**Figure 2.** For the three years, (a) averaged SSC and (b) current velocity in spring tide, (c) depth averaged SSC per station, (d) daily mean averaged discharge in wet season (e) monthly averaged discharge.

The depth-averaged mean current velocity during spring tides in the summer of 2017 was twice as large as that observed in 2016 and 1.5 times greater than the velocity recorded in 2018. The value of neap tides in 2018 was around one-fourth of the value of the spring tides in 2017. The magnitudes of neap tides in 2016 and 2017 were almost half of what was recorded in 2017. During the winter of 2018, the largest depth-averaged current velocity was recorded as  $0.25 \text{ ms}^{-1}$  and  $0.17 \text{ ms}^{-1}$  for spring and neap tide, respectively. The average surface current velocity recorded as  $0.50 \text{ ms}^{-1}$  during the summer spring tide of 2016 was the lowest compared to  $0.63 \text{ ms}^{-1}$  in 2017 and  $0.65 \text{ ms}^{-1}$  in 2018. Conversely, at neap tides, the largest surface current velocity of  $0.56 \text{ ms}^{-1}$  was recorded in 2016. The only wintertime surface current velocity variation was in neap tide, which was higher in 2018 ( $0.36 \text{ ms}^{-1}$ ) than in 2017 ( $0.25 \text{ ms}^{-1}$ ).

In the study area, it was observed that the tidal ranges exhibited their highest and lowest values at the downstream station H. Specifically, the maximum tidal range during the spring tides of 2016 was recorded as 4.51 m, which exceeded the measurements taken in 2017 (4.03 m) and 2018 (4.38 m) [48,49]. In 2018, the downstream station reported the highest tide level, measuring 2.89 m. The largest tidal range observed during neap tides was documented in 2016, measuring 2.83 m at a downstream station.

### 3.2. Surface-Suspended Sediment

Spring tides exhibited a greater number of fluctuations in SSSC compared to neap tides, irrespective of the year and season (Figures 3–5). The highest range of variation (0.28) in along-channel SSSC ( $0.12$  to  $0.40 \text{ kgm}^{-3}$ , as shown in Figure 5a) was seen during spring tides, which was three times more than the highest range of variation ( $0.09$ ) reported during neap tide ( $0.04$  to  $0.13 \text{ kgm}^{-3}$ , as shown in Figure 5b). Similarly, the highest average SSSC measured along the channel during spring tide in winter 2017 was  $0.25 \text{ kgm}^{-3}$ , about three times more than the figure of  $0.09 \text{ kgm}^{-3}$  seen during neap tides in the summer of 2018.

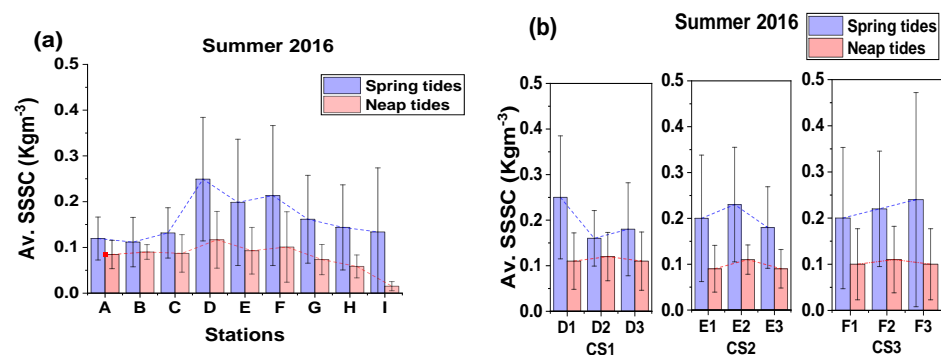


Figure 3. Averaged surface-suspended sediment in summer of 2016 (a) along the channel from stations A to I (b) at the middle-stream.

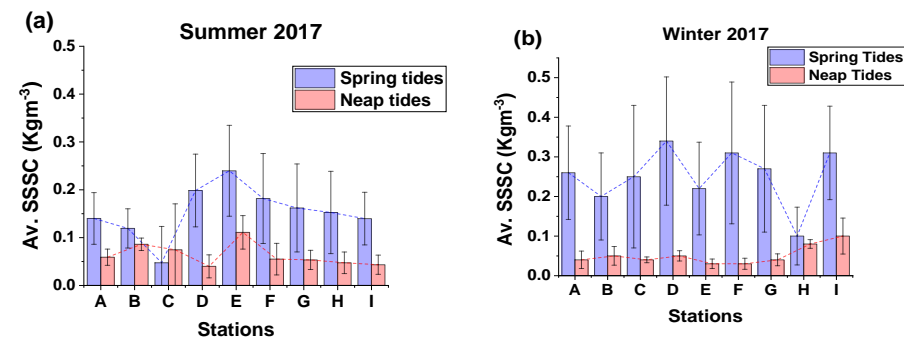


Figure 4. Averaged surface-suspended sediment along channel from stations A to I (a) summer 2017 and (b) winter 2017.

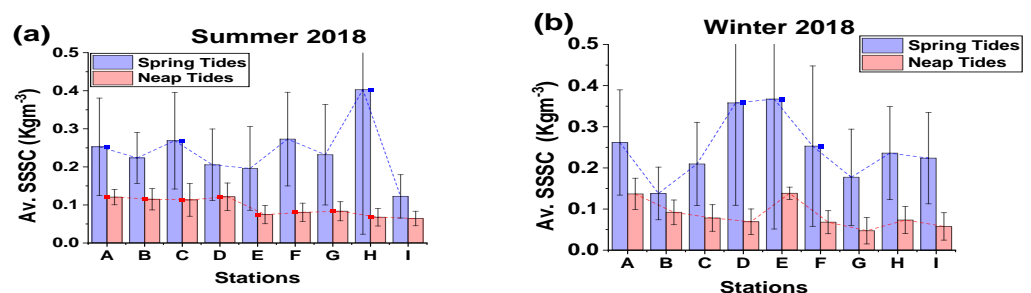


Figure 5. Averaged surface-suspended sediment along the channel from stations A to I (a) summer 2018 and (b) winter 2018.

In summer, the highest range of variance, from 0.12 to 0.40 kgm<sup>-3</sup>, was reported. In contrast, the lowest range, from 0.03 to 0.10 kgm<sup>-3</sup>, was recorded in winter. The maximum along channel DASSSC in summer (0.24 kgm<sup>-3</sup>) did not differ significantly from that in winter (0.25 kgm<sup>-3</sup>). The range of variation in the average SSSC along the channel was greater during winter (0.1 to 0.34 kgm<sup>-3</sup>, as shown in Figure 4b) compared to summer (0.05 to 0.24 kgm<sup>-3</sup>, as shown in Figure 4a) during the spring tides of 2017. In the spring tides of 2018, the range of variance in summer (0.12 to 0.40 kgm<sup>-3</sup>, as shown in Figure 5a) was greater than the range of variation in winter (0.13 to 0.36 kgm<sup>-3</sup>, as shown in Figure 5b).

The SSSC during spring tides in 2017 was 0.15 kgm<sup>-3</sup>, which was lower than the average concentration during winter (0.25 kgm<sup>-3</sup>). However, in 2018, there was no significant variation in SSSC between winter and summer during spring tides, with a concentration of 0.24 kgm<sup>-3</sup>. In 2017, there was no difference in the range of variation between summer (0.04 to 0.11 kgm<sup>-3</sup>, as shown in Figure 4a) and winter (0.03 to 0.1 kgm<sup>-3</sup>, as shown in Figure 4b) during neap tides. However, in 2018, the range of variation in winter (0.04 to 0.13 kgm<sup>-3</sup>, as shown in Figure 5b) was slightly greater than in summer (0.6 to 0.12 kgm<sup>-3</sup>, as shown in Figure 5a).

The highest range of variation (R) in the average along-channel SSSC was reported in 2018 at spring tide, ranging from 0.12 to 0.40 kgm<sup>-3</sup> (see Appendix A Table A3). The average range of SSSC of 0.05 to 0.24 kgm<sup>-3</sup> in 2017 was greater, as shown in Figure 4a and Appendix A Table A2, compared to 0.11 to 0.25 kgm<sup>-3</sup> in 2016, as shown in Figure 3a and Appendix A Table A1.

In neap tides, the 2016 averaged range of SSSC (0.01 to 0.11 kgm<sup>-3</sup>, Appendix A Table A1) showed more variation compared to 2017 (0.04 to 0.11 kgm<sup>-3</sup>, Appendix A Table A2) and 2018 (0.06 to 0.12 kgm<sup>-3</sup>, Appendix A Table A4). During winter, the pattern observed in the spring tide summer remained consistent. The range of SSSC along the channel was greater in 2018 (ranging from 0.14 to 0.37 kgm<sup>-3</sup>, as shown in Appendix A Table A5) compared to 2017 (ranging from 0.10 to 0.31 kgm<sup>-3</sup>, as shown in Appendix A Table A3).

During winter neap tides in 2017 and 2018, the observed magnitudes of SSSC were very low, ranging from 0.03 to 0.1 kgm<sup>-3</sup> in 2017 and from 0.05 to 0.14 kgm<sup>-3</sup> in 2018. The highest along-channel spring tide SSC was recorded in 2018 during the summer season. This was measured at station H, located downstream, with a density of 0.40 kgm<sup>-3</sup>. Station H also had the highest standard deviation of 0.38. During neap tides, there was no significant difference among the three years. In winter, the trend remained consistent, with the year 2018 exhibiting the highest value of 0.37 kgm<sup>-3</sup> during spring tides at the middle reach station E.

When examining the cross-sections in the middle stream, it was found that sub-station D2 had the highest average value of 0.36 kgm<sup>-3</sup> in 2017. On the other hand, the SSSC at sub-station F2 during neap tide varied between 0.051 and 0.091 kgm<sup>-3</sup>, with an average value of 0.082 kgm<sup>-3</sup>. The highest standard deviation of 0.23 was seen in sub-station F3 in 2016 (Figure 3b, Appendix A Table A1).

The highest proportion of aggregates (40% clay), the widest range of D<sub>50</sub> values (4.6 to 10.8 μm), and the highest average surface D<sub>50</sub> value (12 μm) were all seen at neap tide. These findings are illustrated in Figure 6b, station C, and can be further referenced in Tables A6 and A7 in the Appendix A. The spring tide (Table A6 Appendix A) had the highest standard deviation of 3.1. Within the middle stream, the observed standard deviation in the cross-sections reveals increased fluctuations during spring tides, irrespective of the year.

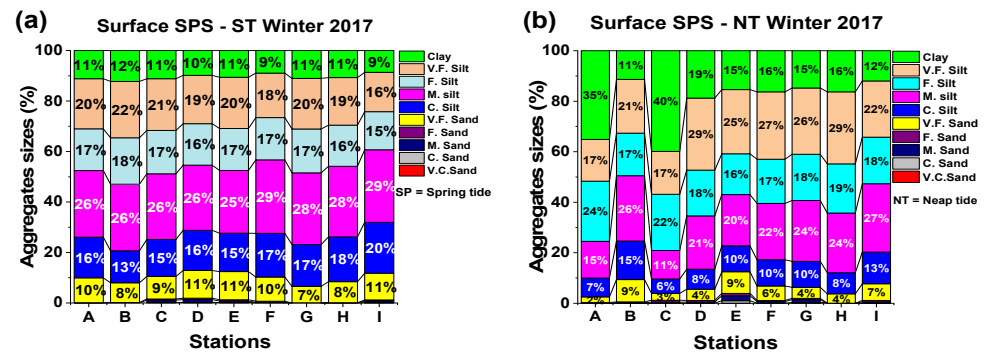


Figure 6. Along-channel surface suspended sediment sizes in winter 2017 (ST: spring tides; NT: neap tides).

### 3.3. Surface Particle Sizes (SPS)

The primary constituent during summer at station G (Figure 7b) is a significant proportion (33%) of very fine silt, but during winter at station C (Figure 6b), clay particles constitute the predominant component (40%). The summer season yielded the highest  $D_{50}$  value, specifically measuring  $12\ \mu\text{m}$ , along with the largest standard deviation of 3.1. These findings are presented in Table A6 of the Appendix A.

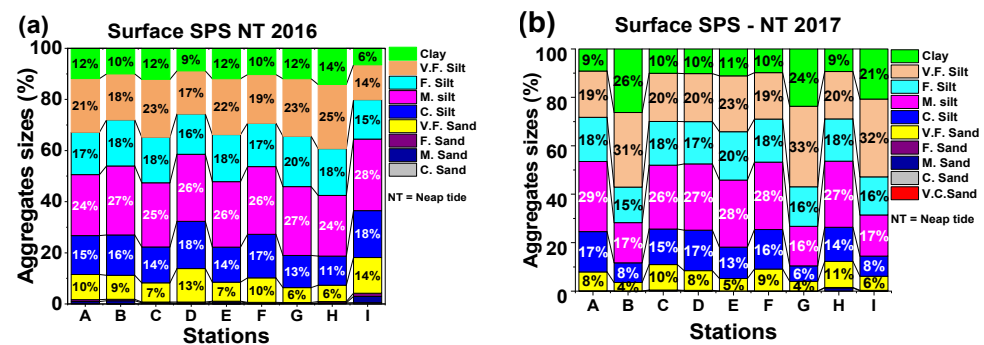


Figure 7. Surface suspended sediment sizes in summer 2016 (a) spring tides and (b) neap tides. Note that the aggregate percentage not present in the figure was too small to be captured during plotting.

In 2016, the average  $D_{50}$  of surface sediments in the channel was from  $7$  to  $12\ \mu\text{m}$  (Figure 8a, Appendix A Table A6). In 2017, the range was from  $4.6$  to  $10.8\ \mu\text{m}$  (Figure 9a, Appendix A Table A7). The quantity of sediment aggregates in 2017 exceeded that in 2016. Significantly, the extremely large-grained sand (VCS) was not documented in the preceding year, 2016. In 2017, a higher concentration of fine particles was reported in the surface water of the middle stream compared to the data from Figure 6 in 2016.

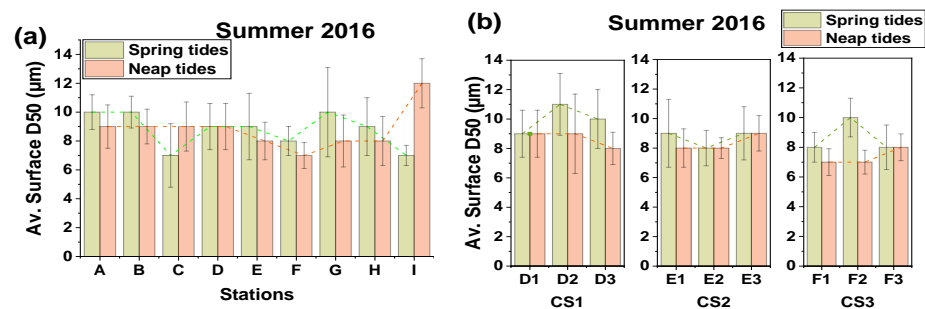
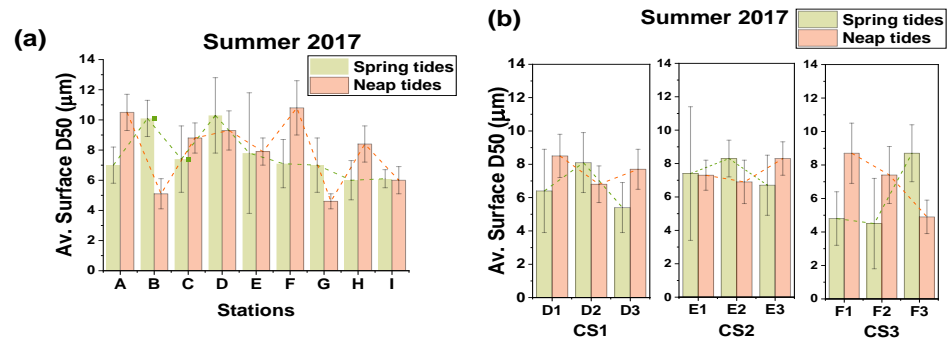


Figure 8. Averaged surface  $D_{50}$  in summer 2016 (a) all along the channel from station A to I, and (b) at the middle stream, along the cross sections, CS1, CS2, and CS3.





**Figure 9.** Averaged surface  $D_{50}$  in summer 2017 (a) all along the channel from station A to I, and (b) and at the middle stream, along the cross sections, CS1, CS2, and CS3.

The average  $D_{50}$  value exhibited greater variability in 2017 (Figure 9b) compared to 2016 (Figure 8b). At CS1, the average surface  $D_{50}$  ranged from 8–11  $\mu\text{m}$  in 2016 to 5.4–8.5  $\mu\text{m}$  in 2017. This information may be found in Tables A6 and A7 in the Appendix A. At CS3, the range of values for the measurement was between 7 and 10  $\mu\text{m}$  in 2016 (Figure 8b, Appendix A Table A6). In 2017, the range of values was between 4.5 and 8.7  $\mu\text{m}$  (refer to the Appendix A, Table A7). The highest  $D_{50}$  value (12  $\mu\text{m}$ ) was documented in 2016; however, the greatest proportion of aggregates was documented in 2017 (31% at CS3, 27% at CS2, and 28% at CS1, refer to Figure A1 in the Appendix A).

In 2016, the percentages of aggregates along the channel were higher than in 2017, with the exception of clay and very fine silt. In 2016, the average surface  $D_{50}$  was below 10  $\mu\text{m}$ , and medium silt was dominant during both neap tides (specifically, 28% at I station) and spring tides (specifically, 28% at G station). In 2017, the middle reach of the area was mostly composed of medium silt. This was particularly evident in neap tides, with percentages of 27%, 28%, and 28% for CS1, CS2, and CS3, respectively (Figure A1 Appendix A).

### 3.4. Surface-Suspended Sediment Concentration

The highest average range during the summer of 2016 (0.17, Figure 10a, with a flooding range of 0.04–0.21  $\text{kgm}^{-3}$ ), the summer of 2017 (0.22, Figure 10b at low slack water, with a range of 0.08–0.30  $\text{kgm}^{-3}$ ), and the winter of 2017 (0.46, Figure 10c at ebb, with a range of 0.15–0.61  $\text{kgm}^{-3}$ ), all occurred during spring tides. Similarly, the highest SSSC (surface suspended sediment concentration) values for summer 2016 (0.23  $\text{kgm}^{-3}$  Figure 10a), summer 2017 (0.30  $\text{kgm}^{-3}$  Figure 10b), and winter 2017 (0.61  $\text{kgm}^{-3}$  Figure 10c) were seen during spring tides. In 2017 (Figure 10b), the highest SSSC values were recorded at ebb tide, mostly at upstream and middle stream stations C and D. Additionally, elevated SSSC values were found during low slack water (LSW), mainly at downstream and middle stream stations G, F, and E. Lastly, increased SSSC values were also noted under flood conditions at station D. The middle channel saw the highest values of SSSC at spring tides (D, E, and F) at LSW in 2016, as shown in Figure 10a.

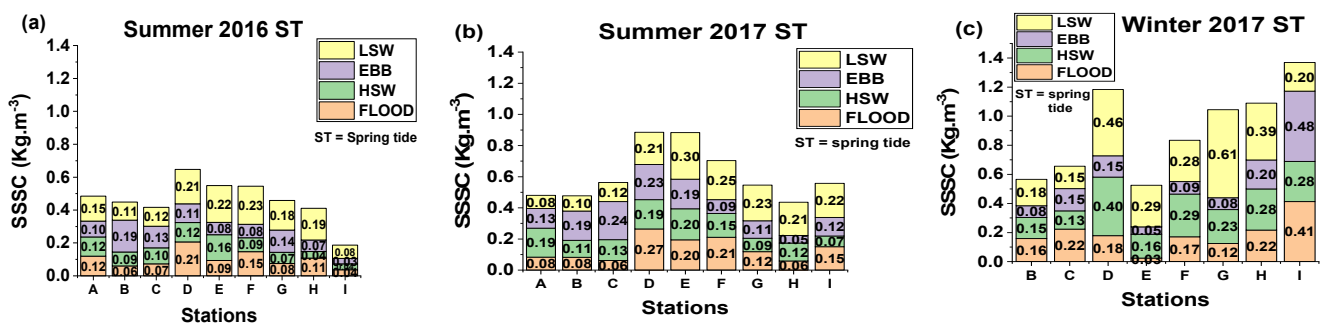


**Figure 10.** Averaged SSSC along the channel in spring tides (a) Summer of 2016; (b) Summer of 2017; (c) Winter of 2017. Note that the data of station A were not recorded in winter of 2017.

### 3.5. Surface Particle Size

The winter season exhibited the highest surface particle size, measuring 11.3  $\mu\text{m}$ , and the largest average range measuring 4.3  $\mu\text{m}$ , during spring tides at ebb, as seen in Figure 11c. In the summer of 2016, the neap tides at LSW had the largest surface particle size (specifically, 13.9  $\mu\text{m}$  at station I) and an average range of 7.4  $\mu\text{m}$  (as shown in Figure 11a). In 2017, the spring tides at LSW had the largest surface particle size (specifically, 15.1  $\mu\text{m}$  at station E) and the largest average range of 10.5  $\mu\text{m}$  (as shown in Figure 11b).

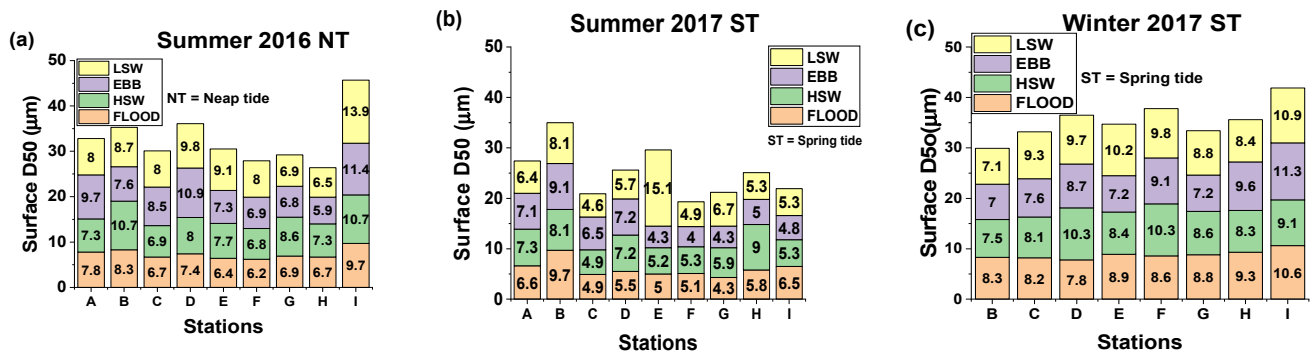


**Figure 11.** Averaged surface  $D_{50}$  in (a) Neap tides (NT) of 2016; (b) Spring tides (ST) of 2017; (c) Spring tide winter of 2017. Note that the data of station A were not recorded in winter of 2017.

## 4. Discussion

### 4.1. Correlations of Hydrological Conditions with SSC and $D_{50}$

The SSC trend of the year 2018 is totally inconsistent with some research results linking water discharge fluctuation to SSC variation [40,41]. More precisely, Figure 2a,c showed a large fluctuation of the daily average and the monthly mean SSC in the three sampling years, respectively, while Figure 2d,e shows the contrary in terms of water discharge. This indicates that water discharge is not behind the large shift observed in SSC variation in 2018; however, it could be explained by the typhoon that occurred this same year [50]. Indeed, the strong winds brought by typhoons significantly enhanced vertical mixing, which had a stronger effect on surface SSC [51,52].

From June 6 to September 16 of 2018, several typhoons occurred around many coastal regions in China, causing huge financial and human losses. The East China Sea and Shanghai coast were involved in these typhoon seasons as well. Moreover, the behavior of the vertical profile of  $D_{50}$  at each tidal phase suggests that the large  $D_{50}$  observed during ebb tide for both years is caused by SSC variations through the tidal discharge and river flow (Figures 10 and 11). However, as indicated by the large standard deviation observed in 2017 and the largest  $D_{50}$  in 2016, it could be possible that the sediment input of the river discharge controlled the  $D_{50}$  size while its flow velocity seemed to control its distribution along the estuary.

### 4.2. Surface-Suspended Sediment

When considering the large range and standard deviation recorded during spring tides for all three observation years, more intra-season variations were observed in spring tide compared to neap tide [50,51]. Estuarine circulation, erosion, resuspension, and vertical mixing are at their maximum display with the strong river discharge, which simultaneously weakens the tidal propagation and damping [27,53]. If this is true in summer, it is not always the case in winter. For instance, the variation range of SSSC and the along channel averaged SSSC in 2017 are larger in winter than in summer. This could be explained by the dry season leading to low water discharge, which allows the tide to become the major hydrodynamic force, playing an important role in salt intrusion and estuary stratification. For instance, the discharge and the surface salinity in winter were 5 times lower and 10 times larger than their value in summer, respectively. The effect of the tide in SSSC seems to be more important than the river discharge, considering the increase in the SSSC at some stations. For instance,

from summer to winter, station C has increased in SSSC five times, meaning that the river discharge is weakening the effect of tide on SSSC. The main hydrodynamic force influencing the upstream stations is the river discharge, which was larger in 2016. Notably, the upstream stations were less affected by tidal currents compared to the middle stream and downstream, which were influenced by a combination of river and tidal discharges. This implies that the downstream stations were most affected by the decrease in tidal discharge during neap tides and winter, resulting in low hydrodynamic activity within the region. As previously noted, the large average SSSC and range recorded in 2018 could be backed up by the typhoon season; however, for 2016 and 2017, it was different, especially in summer neap tide, where 2016 showed large SSSC ranges contrary to the spring tide trend led by 2018. The main reason could reasonably be linked to the 2016 neap tides current velocity and discharge, which did not decrease significantly but were larger than in 2017 and 2018.

The study and observation of the hydrodynamics of the water surface could be an indicator of the ETM location and behavior. For instance, in the summer spring tides of 2016 and 2017, as well as neap tides of 2016 and winter of 2018, the surface sediment had a parabolic shape, increasing from upstream to the middle stations before decreasing towards the downstream direction. As shown in Figures 3a, 4a and 5b, the peak of this parabolic shape representing an area of high SSSC, coincided with stations D, E, and F at the middle channel, which could possibly become an ETM area. This is further realistic since, during spring tide, the standard deviations show a significant variation at the three middle stations, D, E, and F. Moreover, the trend of this SSSC shape follows the depth-averaged SSC trend in the North Passage, meaning that one could use the surface sediment hydrodynamics as a starting point to understand the ETM. Also, the large current velocity, for instance, in neap tide 2017 and in summer 2018, leads to a different pattern, a sinusoidal shape of the SSSC, displaying an irregular distribution (Figures 4b and 5a) with many isolated high SSSC locations, which could be assimilated to the shift in the ETM from one year to another.

The magnitude and the range of SSSC variation in the North Passage seem to be determined by the magnitude of the current velocity, while the sediment load was observed to have a significant impact on the sediment distribution pattern. The middle stream of the channel experienced intense hydrodynamic activities, which could be responsible for the magnitude and the often-large SSSC at the cross-sections (i.e., CS1, CS2, and CS3). Moreover, the middle stream had the largest SSSC where two (i.e., CS1 and CS3) out of the three cross-sections are prone to the formation of estuarine turbidity maximum (ETM). This could be attributed to two major reasons. The magnitude and the range of SSSC variation in the North Passage seem to be determined by the magnitude of the current velocity, while the sediment load was observed to have a significant impact on the sediment distribution pattern [54]. The middle stream of the channel experienced intense hydrodynamic activities, which could be responsible for the magnitude and the often-large SSSC at the cross-sections (i.e., CS1, CS2, and CS3).

Moreover, the middle stream had the largest SSSC where two (i.e., CS1 and CS3) out of the three cross-sections are prone to the formation of estuarine turbidity maximum. This could be attributed to two major reasons. First, the site is located at the salt front with maximum stratification from saline water. Moreover, the density difference between upstream and downstream flow masses, as well as the strong tidal mixing, enhanced the resuspension of suspended sediment [55,56]. Secondly, human activities, such as engineering projects, have had a significant impact on the hydrodynamics condition of the area. For example, the construction of two jetties in this area has drastically altered the sediment dynamics at certain sites in the middle-stream cross-section and along the North Passage. The dredging activities and the deepening of the channel also resulted in increased resuspension of silt and turbidity [51,57].

### 4.3. Surface Particle Sizes

The dominance of neap tides with large aggregate percentages and range variation is still related to the large salinity intrusion in winter 2017 and the low water discharge in the dry season. The along channel averaged salinity recorded in neap tide was even greater than the salinity in summer for the three years. The salinity gradient and tidal mixing could explain the presence of large aggregate percentages and variation ranges of  $D_{50}$  in neap tides, while the sediment transport process is responsible for this dominance in summer since the velocity were still larger. The presence of larger SPS in summer than in winter could be explained by the large water discharge recorded in the wet season, and the large standard deviation recorded in that period confirms that there was a higher hydrodynamics activity in summer than in winter. The clay percentage dominance in winter could also be the result of lower flow velocity from upstream in the dry season since there is no need for large velocity for clay to be resuspended.

Generally, less variation was observed in the averaged  $D_{50}$  of surface sediments in 2016 values compared to 2017. To be precise, while there was less variation of surface averaged  $D_{50}$  between spring and neap tides in 2016, the variation gap was large at several stations in 2017. For instance, in 2016, apart from station I, where the difference of the averaged  $D_{50}$  between spring and neap tides was  $5 \mu\text{m}$  ( $7\text{--}12 \mu\text{m}$ ), the largest averaged  $D_{50}$  difference recorded all along the stations was  $2 \mu\text{m}$  (Figure 8a). Similarly, in 2017, apart from station B with a large difference averaged  $D_{50}$  of  $5 \mu\text{m}$  ( $5.1\text{--}10.1 \mu\text{m}$ ), the variation gap between spring and neap tides was larger than  $2 \mu\text{m}$  at several stations, A (i.e.,  $7 \mu\text{m}$  in neap tide and  $10.5 \mu\text{m}$  in spring tide), F (i.e.,  $7.1 \mu\text{m}$  in neap tide and  $10.8 \mu\text{m}$  in spring tide) and H (i.e.,  $6 \mu\text{m}$  in neap tide and  $8.4 \mu\text{m}$  in spring tide), (Figure 9a). The lower variation in SPS between neap and spring tides in 2016 could be explained firstly by the discharge difference and secondly by the current velocity during these two tidal periods. From spring to neap, the surface current velocity is quite the same, and this behavior of the surface flow can be backed up by the water discharge, which is less variant during the same period. However, the trend is different in 2017, the surface flow and the water discharge clearly reduced from spring to neap. The input of surface flow velocity on SPS is more visible when it comes to tides. In summer, aggregate variations and distributions are dominant during the ebb and LSW along the channel from upstream to downstream, whether spring or neap tides (Figures 10a and 11a). However, the trend is different in winter 2017 (Figures 10c and 11c) for both spring and neap tides. There seems to be a balance in aggregate variations and distributions between landward flow direction (flood and HSW) and seaward flow direction (ebb and LSW). Nevertheless, the variation in aggregates appears to be controlled by the phase of the tide. For instance, in winter aggregates, variations increased according to the flow direction. It increased in the landward direction during flood and HSW and in the seaward direction during ebb and LSW. The combined effect of the turbulent forces created by the motion of the water current during ebb and flood, together with the decreasing flow motion during HSW and LSW, seems to be responsible for these tide-induced aggregate variations [48,58]. In the spring tides of winter 2017, as presented in Figure 11c, aggregates increased seaward for both combinations. In this case, the turbulent forces of upstream flow dominated because the flood season dominated the tidal current flowing upstream.

### 4.4. Tidal Inputs on SSSC and SPS

Regarding the intra-seasonal variation in distribution of SSSC relative to tidal phases, there were clearly more hydrodynamic processes involved during spring than neap tides. However, as previously explained, there seem to be stronger hydrodynamics in winter than in summer since the dry season will weaken the river input while the tide seems to have more of an effect on SSSC variation than river discharge and it's connected hydrodynamic processes. Regardless of the year and season, the low slack water seems to be the most important tidal period because there are always large surface-suspended sediment concentrations and variations at that particular period. The SSSC recorded during low slack water could be the remaining SSSC from ebb resulting from the resuspension of the bottom

deposited sediment by the stronger currents [52,59]. It can be observed that throughout the tidal periods, high SSSC location is slightly shifted in the upstream direction during ebb at stations C, D, and E in spring tides and in stations B and D during neap tides before coming back to its normal area D, E, and F at the other tidal phases, especially in spring tides (Figure 10b). This behavior could be attributed to the shifting in the ETM area under the tidal variations.

In the summer of 2016 (Figures 10a and 11a), ebb and LSW were very important for aggregate distribution and variation, especially during spring tides. Aggregate variations and distributions were dominant during the ebb and LSW along the channel from upstream to downstream, whether spring or neap tides. However, the trend was different in the winter of 2017 (Figures 10c and 11c) for both spring and neap tides.

There seems to be a balance in aggregate variations and distributions between landward flow direction (flood and HSW) and seaward flow direction (ebb and LSW). Nevertheless, the variation in aggregates appear to be controlled by the phase of the tide. For instance, in winter aggregates, variations increased according to the flow direction. It increased in the landward direction during flood and HSW and in the seaward direction during ebb and LSW. The combined effect of the turbulent forces created by the motion of the water current during ebb and flood, together with the decreasing flow motion during HSW and LSW seems to be responsible for these tide-induced aggregate variations [49]. In the spring tides of winter 2017, as presented in Figure 11c), aggregates increased seaward for both combinations. In this case, the turbulent forces of upstream flow dominate because the flood season dominated the tidal current flowing upstream.

The study and analysis of particle SSSC and particle size are useful in assessing ETM [43] and the sediment dynamic variation in the estuary [53]. The present assertion that extreme events significantly impact the sediment dynamic of the estuary corroborates previous findings [27,43,53,54,60]. Even though the methods are different, the outcomes of the present and previous studies highlight the importance of extreme events on estuarine sediment dynamics. Nevertheless, from this study, the variation caused by extreme events on estuarine sediment dynamics is more observable under the tidal cycle and phases.

## 5. Conclusions

Extreme weather conditions are behind the hydrological and sediment dynamic changes in the North Passage of the Yangtze estuary from 2016 to 2018. Surface sediment dynamics can be used as a foundation for comprehending the spatiotemporal variation in ETM in the North Passage of the Yangtze estuary. On account of these hydrological and hydrodynamic differences, more sediment aggregates were recorded in 2017 than in 2016. Medium silt dominated in 2016 and in the winter of 2017, while very fine silt had the largest percentage of SPS recorded in 2017. From 2016 to 2017, there was a slight decrease in surface particle size. More intra-season variations were observed in spring tide compared to neap tide, especially in summer, while in winter, it was the contrary; in winter, the surface hydrodynamics of the neap tide are as important as in the spring tide.

The effect of the tide on SSSC seems to be more important than the river discharge, looking at the increase in the SSSC at some stations, especially for downstream stations in the dry season (winter). However, the main hydrodynamic force influencing the upstream stations in the North Passage is the river discharge, which was larger in 2016.

The intensity and the range of SSSC variation in the North Passage seem to be determined by the magnitude of the current velocity, while the sediment load significantly impacts the sediment distribution pattern.

**Author Contributions:** Conceptualization, Y.C. and S.L.Z.A.; methodology, A.C. and S.L.Z.A.; software, A.C. and S.L.Z.A.; validation, Y.C., A.C. and S.U.O.; formal analysis, G.Z.E. and S.L.Z.A.; investigation, G.A.L.M. and S.L.Z.A.; resources, Y.C. and A.C.; data curation, A.C.; writing—original draft preparation, S.L.Z.A. and S.U.O.; writing—review and editing, S.U.O., S.L.Z.A., Y.C. and A.C.; visualization, S.U.O.; supervision, Y.C. and A.C.; project administration, Y.C.; funding acquisition, Y.C. All authors have read and agreed to the published version of the manuscript.

**Funding:** This work was financially supported by the National R&D Projects of China (No. 2023YFC3008100, 2017YFC0405400) and the Fundamental Research Funds for the Central Universities of Hohai University (HHU-No. 202004017).

**Data Availability Statement:** Restrictions apply to the availability of these data. Data were obtained from the Yangtze River Estuary Water Environment Monitoring Centre and are available (from the authors/at URL) with the permission of the Yangtze River Estuary Water Environment Monitoring Centre.

**Conflicts of Interest:** The authors declare no conflict of interest.

**Appendix A**

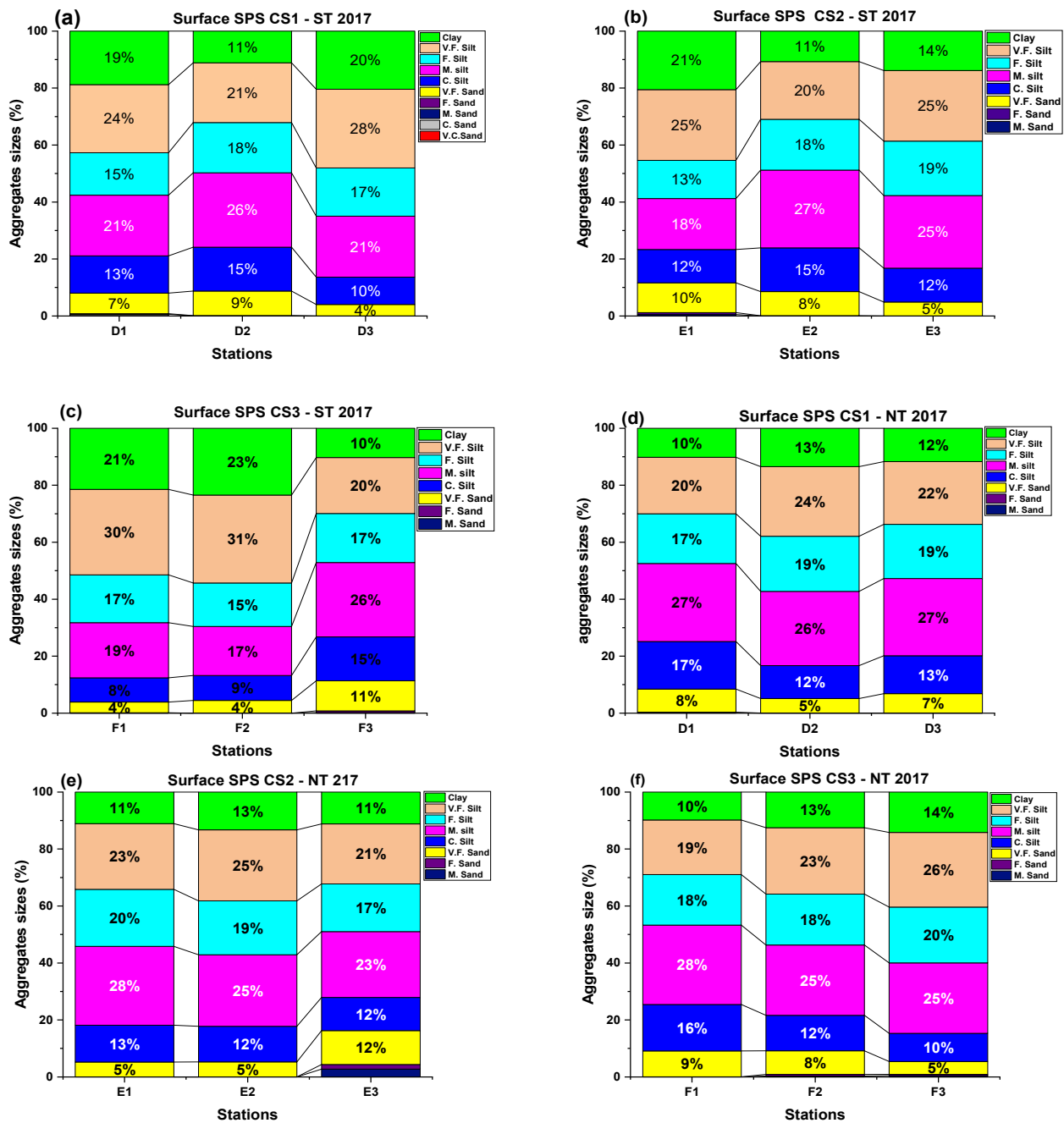


**Figure A1.** Cross-sectional suspended sediment sizes distribution in 2017: Spring tide—(a) Cross-section 1; (b) Cross-section 2; (c) Cross-section 3; Neap tide—(d) Cross-section 1; (e) Cross-section 2; (f) Cross-section 3.

**Table A1.** Averaged SSSC and standard deviation (STD) in summer of 2016 during spring and neap tides along the channel and at the three cross-sections.

Stations	Av. Surface SSC 2016 (Kgm <sup>-3</sup> ) Spring Tides	STD	Av. Surface SSC 2016 (Kgm <sup>-3</sup> ) Neap Tides	STD
A	0.11	0.047	0.08	0.03
B	0.11	0.054	0.09	0.01
C	0.13	0.055	0.08	0.04
D	0.24	0.135	0.11	0.06
E	0.19	0.138	0.09	0.05
F	0.21	0.153	0.10	0.07
G	0.16	0.096	0.07	0.03
H	0.14	0.093	0.05	0.02
I	0.13	0.14	0.01	0.01
CS1				
D1	0.25	0.135	0.11	0.062
D2	0.16	0.061	0.12	0.053
D3	0.18	0.102	0.11	0.064
CS2				
E1	0.2	0.138	0.09	0.051
E2	0.23	0.125	0.11	0.032
E3	0.18	0.089	0.09	0.042
CS3				
F1	0.2	0.153	0.1	0.077
F2	0.22	0.125	0.11	0.072
F3	0.24	0.232	0.1	0.077

**Table A2.** Averaged SSSC and standard deviation (STD) in summer 2017 during spring and neap tides along the channel and at the three cross-sections.

Stations	Av. Surface SSC 2017 (Kgm <sup>-3</sup> ) Summer-Spring Tides	STD	Av. Surface SSC 2017 (Kgm <sup>-3</sup> ) Summer-Neap Tides	STD
A	0.14	0.05	0.06	0.01
B	0.12	0.04	0.09	0.01
C	0.05	0.07	0.07	0.09
D	0.20	0.07	0.04	0.02
E	0.24	0.09	0.11	0.03
F	0.18	0.09	0.05	0.03
G	0.16	0.09	0.05	0.02
H	0.15	0.08	0.05	0.02
I	0.14	0.05	0.04	0.02
CS1				
D1	0.2	0.076	0.39	0.024
D2	0.36	0.143	0.118	0.066
D3	0.19	0.073	0.121	0.043
CS2				
E1	0.23	0.1	0.11	0.035
E2	0.19	0.07	0.06	0.034
E3	0.18	0.06	0.08	0.03
CS3				
F1	0.176	0.09	0.05	0.03
F2	0.23	0.095	0.08	0.04
F3	0.206	0.26	0.07	0.07

**Table A3.** Averaged SSSC and standard deviation (STD) in winter 2017 during spring and neap tides along the channel.

Stations	Av. Surface SSC 2017 (Kgm <sup>-3</sup> ) Winter-Spring Tides	STD	Av. Surface SSC 2017 (Kgm <sup>-3</sup> ) Winter-Neap Tides	STD
A	0.26	0.11	0.04	0.02
B	0.20	0.11	0.05	0.02
C	0.25	0.18	0.04	0.007
D	0.34	0.16	0.05	0.013
E	0.22	0.11	0.03	0.012
F	0.31	0.17	0.03	0.014
G	0.27	0.16	0.04	0.015
H	0.10	0.07	0.08	0.011
I	0.31	0.11	0.10	0.045

**Table A4.** Averaged SSSC in summer 2018 along the channel during spring and neap tides.

Stations	Averaged Surface SSC (Kgm <sup>-3</sup> ) Summer-Spring Tides 2018	STD	Averaged Surface SSC (Kgm <sup>-3</sup> ) Summer-Neap Tides 2018	STD
A	0.25	0.12	0.12	0.02
B	0.22	0.067	0.11	0.028
C	0.27	0.12	0.11	0.04
D	0.21	0.09	0.12	0.036
E	0.20	0.11	0.07	0.024
F	0.27	0.12	0.08	0.024
G	0.23	0.13	0.08	0.025
H	0.40	0.38	0.07	0.023
I	0.12	0.05	0.06	0.02

**Table A5.** Averaged SSSC in winter 2018 along the channel during spring and neap tides.

Stations	Averaged Surface SSC 2018 (Kgm <sup>-3</sup> ) Winter-Spring Tides	STD	Averaged Surface SSC 2018 (Kgm <sup>-3</sup> ) Winter-Neap Tides	STD
A	0.26	0.128	0.14	0.038
B	0.14	0.06	0.09	0.03
C	0.21	0.10	0.08	0.032
D	0.36	0.24	0.07	0.031
E	0.37	0.31	0.14	0.015
F	0.25	0.19	0.07	0.028
G	0.18	0.11	0.05	0.032
H	0.24	0.11	0.07	0.033
I	0.22	0.11	0.06	0.033



**Table A6.** Averaged surface  $D_{50}$  in summer 2016 along the channel and at the middle stream during spring and neap tides.

Stations	Averaged Surface $D_{50}$ ( $\mu\text{m}$ ) 2016 Spring Tides	STD	Averaged Surface $D_{50}$ ( $\mu\text{m}$ ) 2016 Neap Tides	STD
A	10	1.2	9	1.5
B	10	1.1	9	1.2
C	7	2.2	9	1.7
D	9	1.6	9	1.6
E	9	2.3	8	1.3
F	8	1	7	0.9
G	10	3.1	8	1.8
H	9	2	8	1.7
I	7	0.7	12	1.7
CS1				
D1	9	1.6	9	1.6
D2	11	2.1	9	2.7
D3	10	2	8	1.1
CS2				
E1	9	2.3	8	1.3
E2	8	1.2	8	0.7
E3	9	1.8	9	1.2
CS3				
F1	8	1	7	0.9
F2	10	1.3	7	0.8
F3	8	1.5	8	0.9

**Table A7.** Averaged surface  $D_{50}$  in the summer 2017 along the channel and at the middle stream during spring and neap tides.

Stations	Averaged Surface $D_{50}$ ( $\mu\text{m}$ ) 2017 Spring Tides	STD	Averaged Surface $D_{50}$ ( $\mu\text{m}$ ) 2017 Neap Tides	STD
A	7	1.2	10.5	1.2
B	10.1	1.2	5.1	1
C	7.4	2.2	8.8	1
D	10.3	2.5	9.3	1.3
E	7.8	4	7.9	0.9
F	7.1	1.6	10.8	1.8
G	7	1.8	4.6	0.5
H	6	1.3	8.4	1.2
I	6.1	0.6	6	0.9
CS1				
D1	6.4	2.5	8.5	1.3
D2	8.1	1.8	6.8	1.1
D3	5.4	1.5	7.7	1.2
CS2				
E1	7.4	4	7.3	0.9
E2	8.3	1.1	6.9	1.3
E3	6.7	1.8	8.3	1
CS3				
F1	4.8	1.6	8.7	1.8
F2	4.5	2.7	7.4	1.7
F3	8.7	1.7	4.9	1

## References

- Latrubesse, E.M.; Park, E.; Lim, J. Geomorphology and Suspended Sediment Transport of the Second Largest River of Southeast Asia: The Irrawaddy River, Myanmar. In *AGU Fall Meeting Abstracts*; AA (Nanyang Technological University): Singapore; AB (University of Texas at Austin): Austin, TX, USA; AC (Nanyang Technological University): Singapore, 2019; Volume 2019, p. EP51E-2120. Available online: <https://ui.adsabs.harvard.edu/abs/2019AGUFMEP51E2120L> (accessed on 1 December 2023).
- ywater-Reyes, S.; Segura, C.; Bladon, K.D. Geology and geomorphology control suspended sediment yield and modulate increases following timber harvest in temperate headwater streams. *J. Hydrol.* **2017**, *548*, 754–769. [[CrossRef](#)]
- Chu, A. *Analysis and Modelling of Morphodynamics of the Yangtze Estuary*; Delft University of Technology: Delft, The Netherlands, 2019.
- Rodgers, K.; McLellan, I.; Peshkur, T.; Williams, R.; Tonner, R.; Knapp, C.W.; Henriquez, F.L.; Hursthouse, A.S. The legacy of industrial pollution in estuarine sediments: Spatial and temporal variability implications for ecosystem stress. *Environ. Geochem. Health* **2019**, *42*, 1057–1068. [[CrossRef](#)] [[PubMed](#)]
- Zhang, W.; Xu, Y.J.; Guo, L.; Lam, N.S.-N.; Xu, K.; Yang, S.; Yao, Q.; Liu, K.-B. Comparing the Yangtze and Mississippi River Deltas in the light of coupled natural-human dynamics: Lessons learned and implications for management. *Geomorphology* **2022**, *399*, 108075. [[CrossRef](#)]
- Yang, H.-B.; Li, E.-C.; Zhao, Y.; Liang, Q.-H. Effect of water-sediment regulation and its impact on coastline and suspended sediment concentration in Yellow River Estuary. *Water Sci. Eng.* **2017**, *10*, 311–319. [[CrossRef](#)]
- Yufang, H.; Chuanteng, L. Process research on estuarine turbidity maximum and mouth bar of Yangtze Estuary after the improvement works. *Procedia Eng.* **2015**, *116*, 80–87. [[CrossRef](#)]
- Jie, J.; Qing, H.; Lei, Z.; Lin, J. Analysis of hydrodynamic features of the north passage in the turbidity maximum, Changjiang estuary. *Haiyang Xuebao* **2019**, *41*, 11–20. [[CrossRef](#)]
- Shen, F.; Salama, M.S.; Zhou, Y.-X.; Li, J.-F.; Su, Z.; Kuang, D.-B. Remote-sensing reflectance characteristics of highly turbid estuarine waters—A comparative experiment of the Yangtze River and the Yellow River. *Int. J. Remote Sens.* **2010**, *31*, 2639–2654. [[CrossRef](#)]
- Song, D.; Dong, Y.; Bao, X. Spring-neap tidal variation and mechanism analysis of the maximum turbidity in the Pearl River Estuary during flood season. *J. Trop. Oceanogr.* **2020**, *39*, 20–35. Available online: <https://www.sciengine.com/JTO/doi/10.11978/2019035;JSESSIONID=7878deba-6c18-4eed-9798-3e4907955e88> (accessed on 1 December 2023).
- Boyd, C.E. *Particulate Matter, Turbidity, and Color BT—Water Quality: An Introduction*; Boyd, C.E., Ed.; Springer: Boston, MA, USA, 2000; pp. 95–103. [[CrossRef](#)]
- Xu, F.; Yao, J.; Tao, J.F.; Yang, T. Effect of Large Scale Tidal Flat Reclamation on Hydrodynamic Circulation in Jiangsu Coastal Areas. In *Asian and Pacific Coasts*; 2011; pp. 662–669. Available online: [https://www.worldscientific.com/doi/abs/10.1142/9789814366489\\_0077%20heart%201](https://www.worldscientific.com/doi/abs/10.1142/9789814366489_0077%20heart%201) (accessed on 1 December 2023).
- Chen, X.Q.; Yan, Y.X.; Dou, X.P. Preliminary Analysis of the Effects on the Yangtze Estuary After Three-Gorge Project Operation. In *Proceedings of the 6th International Conference on APAC 2011, Asian and Pacific Coasts*, Hong Kong, 14–16 December 2011.
- Wilson, P.C. Water Quality Notes: Water Clarity (Turbidity Suspended Solids and Color) 1. *Dep. Soil Water Ecosyst. Sci.* **2013**, *SL314*, 1–8. Available online: <https://web.archive.org/web/20200709172438/https://edis.ifas.ufl.edu/pdffiles/SS/SS52600.pdf> (accessed on 1 December 2023).
- Shen, F.; Verhoef, W.; Zhou, Y.; Salama, M.S.; Liu, X. Satellite Estimates of Wide-Range Suspended Sediment Concentrations in Changjiang (Yangtze) Estuary Using MERIS Data. *Estuaries Coasts* **2010**, *33*, 1420–1429. [[CrossRef](#)]
- Chen, H.; Zhang, J.; Wang, S.; Sun, D.; Qiu, Z. Study on diurnal variation of turbidity in the Yangtze Estuary and adjacent areas by remote sensing. *Acta Opt. Sin.* **2020**, *40*, 501003. [[CrossRef](#)]
- Wang, C.; Wang, D.; Yang, J.; Fu, S.; Li, D. Suspended Sediment within Estuaries and along Coasts: A Review of Spatial and Temporal Variations based on Remote Sensing. *J. Coast. Res.* **2020**, *36*, 1323–1331. [[CrossRef](#)]
- Wan, Y.; Wang, L. Study on the seasonal estuarine turbidity maximum variations of the Yangtze estuary, China. *J. Waterw. Port Coast. Ocean. Eng.* **2018**, *144*, 5018002. [[CrossRef](#)]
- Xu, H.-J.; Huang, Z.; Bai, Y.-C.; Su, L.-S.; Hong, Y.-C.; Lu, T.-T.; Wang, X. Numerical analysis of sediment deposition in Yangtze river estuary: Insight from conceptual estuary models. *Appl. Ocean Res.* **2020**, *104*, 102372. [[CrossRef](#)]
- Shu, C.; Tan, G.; Lv, Y.; Xu, Q. Field methods of a near-bed suspended sediment experiment in the Yangtze River, China. *Arab. J. Geosci.* **2020**, *13*, 1118. [[CrossRef](#)]
- Yang, H.; Li, B.; Zhang, C.; Qiao, H.; Liu, Y.; Bi, J.; Zhang, Z.; Zhou, F. Recent Spatio-Temporal Variations of Suspended Sediment Concentrations in the Yangtze Estuary. *Water* **2020**, *12*, 818. [[CrossRef](#)]
- Wu, S.; Cheng, H.; Xu, Y.J.; Li, J.; Zheng, S.; Xu, W. Riverbed Micromorphology of the Yangtze River Estuary, China. *Water* **2016**, *8*, 190. [[CrossRef](#)]
- Wu, S.; Cheng, H.; Xu, Y.; Li, J.; Zheng, S. Decadal changes in bathymetry of the Yangtze River Estuary: Human impacts and potential saltwater intrusion. *Estuar. Coast. Shelf Sci.* **2016**, *182*, 158–169. [[CrossRef](#)]
- Tang, M.; Cheng, H.; Xu, Y.; Hu, H.; Zheng, S.; Wang, B.; Yang, Z.; Teng, L.; Xu, W.; Zhang, E.; et al. Channel Bed Adjustment of the Lowermost Yangtze River Estuary from 1983 to 2018: Causes and Implications. *Water* **2022**, *14*, 4135. [[CrossRef](#)]
- Teng, L.; Cheng, H.; de Swart, H.; Dong, P.; Li, Z.; Li, J.; Wang, Y. On the mechanism behind the shift of the turbidity maximum zone in response to reclamations in the Yangtze (Changjiang) Estuary, China. *Mar. Geol.* **2021**, *440*, 106569. [[CrossRef](#)]

26. Silva, A.M.M.; Asp, N.E.; Gomes, V.J.C.; Ogston, A.S. Impacts of Inherited Morphology and Offshore Suspended-Sediment Load in an Amazon Estuary. *Estuaries Coasts* **2023**, *46*, 1709–1722. [CrossRef]
27. Silva, A.M.M.; Glover, H.E.; Josten, M.E.; Gomes, V.J.C.; Ogston, A.S.; Asp, N.E. Implications of a Large River Discharge on the Dynamics of a Tide-Dominated Amazonian Estuary. *Water* **2023**, *15*, 849. [CrossRef]
28. Folk, R.L. A Review of Grain-Size Parameters. *Sedimentology* **1966**, *6*, 73–93. [CrossRef]
29. Guo, L.; Su, N.; Townend, I.; Wang, Z.B.; Zhu, C.; Wang, X.; Zhang, Y.; He, Q. From the headwater to the delta: A synthesis of the basin-scale sediment load regime in the Changjiang River. *Earth-Sci. Rev.* **2019**, *197*, 102900. [CrossRef]
30. Chen, N.; Krom, M.D.; Wu, Y.; Yu, D.; Hong, H. Storm induced estuarine turbidity maxima and controls on nutrient fluxes across river-estuary-coast continuum. *Sci. Total. Environ.* **2018**, *628–629*, 1108–1120. [CrossRef] [PubMed]
31. Peng, T.; Tian, H.; Singh, V.P.; Chen, M.; Liu, J.; Ma, H.; Wang, J. Quantitative assessment of drivers of sediment load reduction in the Yangtze River basin, China. *J. Hydrol.* **2020**, *580*, 124242. [CrossRef]
32. Zhu, C.; Zhang, Y.; van Maren, D.S.; Xie, W.; Guo, L.; Wang, X.; He, Q. Modulation of sediment load recovery downstream of Three Gorges Dam in the Yangtze River. *Anthr. Coasts* **2023**, *6*, 2. [CrossRef]
33. Wang, C.; Wang, H.; Song, G.; Zheng, M. Grain size of surface sediments in Selin Co (central Tibet) linked to water depth and offshore distance. *J. Paleolimnol.* **2019**, *61*, 217–229. [CrossRef]
34. Fang, D.; Sun, H.; Peng, Y.; Kuang, Z.; Zhou, Y.; Xu, D. Living Status and Perspective of the Silver Carp (*Hypophthalmichthys molitrix*) in the Lower Reach of the Yangtze River: Insights from Population Distribution, Age Structure, and Habitat Preference Analyses. *Fishes* **2022**, *7*, 254. [CrossRef]
35. Strickland, J.D.H.; Parsons, T.R. *A Practical Handbook of Seawater Analysis*; Fisheries Research Board of Canada: Ottawa, ON, Canada, 1972.
36. Li, W.; Jiang, C.; Zuo, S.; Li, J. Human Intervention-Induced Changes in the Characteristics of the Turbidity Maximum Zone and Associated Mouth Bars in the Yangtze Estuary. *J. Mar. Sci. Eng.* **2022**, *10*, 584. [CrossRef]
37. Li, W.; Li, M.; Zhang, X.; Li, J. Characteristics of fluid mud in the Yangtze Estuary: Storm, tide, and slope-triggered sediment dynamics and effects. *Estuar. Coast. Shelf Sci.* **2023**, *281*. [CrossRef]
38. Chen, J. ADP-flow velocity profile to interpret hydromorphological features of China's Yangtze Three-Gorges valley. *Chin. Sci. Bull.* **2005**, *50*, 679. [CrossRef]
39. Chen, J.Y.; Shen, H.T.; Yun, C.X. *Dynamic Processes and Morphological Evolution of the Changjiang Estuary*; Shanghai Science and Technology Press: Shanghai, China, 1988.
40. Huang, Y.-G.; Yang, H.-F.; Jia, J.-J.; Li, P.; Zhang, W.-X.; Wang, Y.P.; Ding, Y.-F.; Dai, Z.-J.; Shi, B.-W.; Yang, S.-L. Declines in suspended sediment concentration and their geomorphological and biological impacts in the Yangtze River Estuary and adjacent sea. *Estuar. Coast. Shelf Sci.* **2022**, *265*, 107708. [CrossRef]
41. Fan, H.; Yan, H.; Teng, L.; Liu, R.; Li, Z.; Cheng, H.; Zhang, E. The effects of extreme flood events on the turbidity maximum zone in the Yangtze (Changjiang) Estuary, China. *Mar. Geol.* **2023**, *456*, 106993. [CrossRef]
42. Shepard, F.P. Nomenclature Based on Sand-silt-clay Ratios. *J. Sediment. Res.* **1954**, *24*, 151–158. Available online: <https://api.semanticscholar.org/CorpusID:129806833> (accessed on 1 December 2023).
43. Version, A.F.; Soils, C.O.F.; The, F.O.R.; Dredging, M. WG Report n° 144-2017 Abridged Field Version Classification of Soils and Rocks for the Maritime Dredging Process. 2017. Available online: <https://izw.baw.de/publikationen/pianc/0/marcom144.pdf> (accessed on 1 December 2023).
44. Oladipo, V.O.; Adedoyin, A.D.; Atat, J.G. The Geostatistical Investigation of Grain Size and Heavy Minerals of Stream Sediments from Agunjin Area, Kwara State. *World J. Appl. Sci. Technol.* **2018**, *10*, 249–257.
45. Pareja-Roman, L.F.; Orton, P.M.; Talke, S.A. Effect of Estuary Urbanization on Tidal Dynamics and High Tide Flooding in a Coastal Lagoon. *J. Geophys. Res. Oceans* **2023**, *128*, e2022JC018777. [CrossRef]
46. Sohrt, V.; Hein, S.S.; Nehlsen, E.; Strotmann, T.; Fröhle, P. Model Based Assessment of the Reflection Behavior of Tidal Waves at Bathymetric Changes in Estuaries. *Water* **2021**, *13*, 489. [CrossRef]
47. Fivash, G.S.; Temmerman, S.; Kleinhans, M.G.; Heuner, M.; van der Heide, T.; Bouma, T.J. Early indicators of tidal ecosystem shifts in estuaries. *Nat. Commun.* **2023**, *14*, 1911. [CrossRef]
48. Wang, H.; Jia, Y.; Ji, C.; Jiang, W.; Bian, C. Internal tide-induced turbulent mixing and suspended sediment transport at the bottom boundary layer of the South China Sea slope. *J. Mar. Syst.* **2022**, *230*, 103723. [CrossRef]
49. Xing, F.; Wang, Y.P.; Jia, J. Hydrodynamics and sediment transport patterns on intertidal flats along middle Jiangsu coast. *Anthr. Coasts* **2022**, *5*, 1–19. [CrossRef]
50. Huang, J.; Zhu, J. Suspended sediment dynamics and influencing factors during typhoons in Hangzhou Bay, China. *Anthr. Coasts* **2023**, *6*, 3. [CrossRef]
51. Essink, K. Ecological effects of dumping of dredged sediments; options for management. *J. Coast. Conserv.* **1999**, *5*, 69–80. [CrossRef]
52. Li, Z.; Wang, Y.; Cheng, P.; Zhang, G.; Li, J. Flood-ebb asymmetry in current velocity and suspended sediment transport in the Changjiang Estuary. *Acta Oceanol. Sin.* **2016**, *35*, 37–47. [CrossRef]
53. Xiao, C.; Zhu, X.-H.; Zhang, C.; Zhu, Z.-N.; Ma, Y.L.; Zhong, J.W.; Wei, L.X. Coastal acoustic tomography system for monitoring transect suspended sediment discharge of Yangtze river. *J. Hydrol.* **2023**, *623*, 129832. [CrossRef]

54. Wolanski, E.; Gibbs, R.J.; Mazda, Y.; Mehta, A.; King, B. The Role of Turbulence in the Settling of Mud Flocs. *J. Coast. Res.* **1992**, *8*, 35–46. Available online: <http://www.jstor.org/stable/4297950> (accessed on 1 December 2023).
55. Zhu, C.; van Maren, D.S.; Guo, L.; Lin, J.; He, Q.; Wang, Z.B. Effects of Sediment-Induced Density Gradients on the Estuarine Turbidity Maximum in the Yangtze Estuary. *J. Geophys. Res. Oceans* **2021**, *126*, e2020JC016927. [[CrossRef](#)]
56. Vinh, V.D.; Ouillon, S.; Van Uu, D. Estuarine Turbidity Maxima and Variations of Aggregate Parameters in the Cam-Nam Trieu Estuary, North Vietnam, in Early Wet Season. *Water* **2018**, *10*, 68. [[CrossRef](#)]
57. Yang, Z.F.; Chen, D.; Xiao, B.P. Impact assessment of dredging on fish eggs and larvae: A case study in Caotan, South China. *IOP Conf. Ser. Earth Environ. Sci.* **2019**, *351*, 012035. [[CrossRef](#)]
58. Zhang, Y.; Ren, J.; Zhang, W.; Wu, J. Importance of salinity-induced stratification on flocculation in tidal estuaries. *J. Hydrol.* **2021**, *596*, 126063. [[CrossRef](#)]
59. Teng, L.; Cheng, H.; Zhang, E.; Wang, Y. Lateral Variation of Tidal Mixing Asymmetry and Its Impact on the Longitudinal Sediment Transport in Turbidity Maximum Zone of Salt Wedge Estuary. *J. Mar. Sci. Eng.* **2022**, *10*, 907. [[CrossRef](#)]
60. Allen, R.M.; Lacy, J.R.; Stacey, M.T.; Variano, E.V. Seasonal, Spring-Neap, and Tidal Variation in Cohesive Sediment Transport Parameters in Estuarine Shallows. *J. Geophys. Res. Ocean.* **2019**, *124*, 7265–7284. [[CrossRef](#)]

**Disclaimer/Publisher’s Note:** The statements, opinions and data contained in all publications are solely those of the individual author(s) and contributor(s) and not of MDPI and/or the editor(s). MDPI and/or the editor(s) disclaim responsibility for any injury to people or property resulting from any ideas, methods, instructions or products referred to in the content.